INVESTIGATIONS ON THE SWIRL FLOW CAUSED BYAN AXIAL FAN: A CONTRIBUTION TO THE REVISION OFISO 5801

Philipp MATTERN[1], Sten SIEBER[1], Đorđe ČANTRAK[2], Friedrich FRÖHLIG[1], ŞabanÇAĞLAR[1], Martin GABI[1]

[1]*Institute of Fluid Machinery (FSM), Karlsruhe Institute of Technology (KIT), Kaiserstraße 12,76131 Karlsruhe, GERMANY*

[2]*Hydraulic Machinery and Energy Systems Department, Faculty of Mechanical Engineering, University of Belgrade, KraljiceMarije 16, 11120 Belgrade 35, SERBIA*

SUMMARY

This paper deals with the incompressible turbulent swirl flow behind an axial fan without guide vanes in a straight circular duct. The authors used High-Speed-Stereo-Particle Image Velocimetry (HSS-PIV) to visualise and quantify the flow in the duct downstream an axial fan. The intention was to document and to help young engineers understanding the complex flow pattern. The presented energy loss coefficients for a swirl flow along a straight circular duct could be used to complement the calculation of the loss allowances in ISO 5801.

INTRODUCTION

Investigation of the turbulent swirl flow in technical practice is of great significance. Whilst this paper examines this complex fluid flow phenomenon, the aim is to apply the conclusions to the revision of the ISO 5801:2007 standard "*Industrial fans – Performance testing using standardized airways*" [1]. In this study, the test rig had a free bell-mouth inlet and a ducted outlet, and resembled a Category B installation in ISO 5801. The paper presents laser-optical measurements of the velocity field at the axial fan pressure side, without outlet guide vanes. High-Speed-Stereo-Particle Image Velocimetry (HSS-PIV) measurements were carried out in a cross sectional plane and in a plane including the duct axis.

In a thesis on the swirl flow in a circular duct with integral classical measuring techniques, Vasilescu [2] used adjustable guide vanes to generate a swirl at the duct inlet. He examined the hub's influence by introducing pipes of various diameters so that he could technically obtain different non-dimensional parameters, i.e. hub ratio ν values.This allowed geometric observation of the flow that suddenly

changed from an annulus to a circular shape. Known as a “Carnot annular diffuser”, this also occurs in axial turbo machines. Kinetic energy recuperationin such a geometry results in the static wall pressure greatly increasing. The"optimum length" of the diffuser for the maximum wall pressure recovery is a function of the hub ratio *v* and the swirl intensity at the fan outlet. It is possible to derive from Vasilescu's results[2] an optimum length of the “Carnot annular diffuser” for the design point of axial fans without outlet guide vanes.

In [3] the authors investigated combinations of swirl intensity and hub ratios which usually exist at the axial fan’s design point. They also included cases without a hub. This is of great importance, as the large flow energy loss occurs in the connecting duct. The swirl loss coefficient, in some cases, exceeded more than 100 times the axial flow’s corresponding coefficient.The authors [3] obtained results for the wall pressure distribution from experiments and provide the formula for determining the swirling flow energy loss coefficient [3, 4] which this paper discusses later.

The common segment airways for installations of category B (free inlet and ducted outlet) in ISO 5801 always must incorporate a standardised flow straightener, even when the average total velocity’s angle is less than 15 degrees to the pipe axis. Chapter 28.4 of ISO 5801, “Outlet duct simulation”, mentions the possibility to measure fan performance with a duct of *2D* without a straightener, where *D*is the hydraulic diameter. Chapter 28.6, “Loss allowances for standardizedairways”, provides losses based on fully developed flow in smooth ducts. This incorporates adequate mistakes.

List of Symbols

B	[-]	Decay parameter of the swirl parameter W, introduced in [4]
$\overline{c_m}$	[m/s]	Averaged axial velocity, Eq. (1)
c_{mag}	[m/s]	Velocity magnitude
c_m	[m/s]	Axial velocity component
c_r	[m/s]	Radial velocity component
c_u	[m/s]	Circumferential velocity component
D	[m]	Inner diameter of the duct
D_a	[m]	Outer diameter of the impeller
D_{Hub}	[m]	Hub diameter of the impeller
M_W	[Nm]	Angular momentum, Eq. (7), introduced in [3]
N	[rpm]	Rotational Speed
Δp	[Pa]	Pressure raise
PHI	[-]	Volume flow coefficient: $PHI = \frac{4\dot{V}}{{D_a}^2 \pi u}$
PSI	[-]	Pressure coefficient: $PSI = \frac{2\Delta p}{\rho u^2}$
R	[m]	Radial coordinate
R	[m]	Inner Radius of the duct
R_a	[m]	D_a / 2
Re	[-]	Reynolds number
U	[m/s]	Circumferential velocity of the impeller at D_a
U_m	[m/s]	Averaged axial velocity in a pipe
$\dot{V}$	[m³/s]	Volume flow
W	[-]	Swirl parameter, Eq. (6), introduced in [3]
$\bar{Y}_t$	[m²/s²]	Energy of the flow, Eq.(2)
$\bar{Y}_{tr}$	[m²/s²]	Energy of a swirl flow Eq.(3)
Z	[m]	Axial coordinate along a pipe
z^*	[-]	Non-dimenstional axial coordinate $z^* = z/ R_a$
β_a	[°]	Blade angle at D_a
$\bar{\Gamma}$	[-]	Swirl flow parameter, Eq. (5), introduced in [3]

Λ	[-]	Friction factor for axial flow
λ_Γ	[-]	Energy loss coefficient for swirling flow along a straight circular duct
	[kg/m³]	Density
N	[-]	Ratio of D_{Hub} / D_a
Φ_0	[-]	Swirl flow parameter, introduced in [3]
	[-]	Swirl flow parameter, Eq. (5), introduced in [3]

EXPERIMENTAL INSTALLATIONS

Test setup and fan

Figure 1 illustrates the experimental installation. It shows an acrylic glass duct for the PIV measurements followed by aluminum ducts with an overall length of *20D*. The flexible exhaust hose conducts the flow into a test rig installation consisting of a venturi flowmeter, a choke and a booster.

For the measurement of the characteristic curve of the fan, the acrylic glass duct was replaced by an aluminum duct, equipped with an array of 12 independent pressure sensors. Here this measurement was only used to get the characteristic curve of the axial fan.
To verify the operation point during PIV measurements, the author measured the wall pressure, averaged from four points in a cross section *5D* downstream from the trailing edge of the blade.

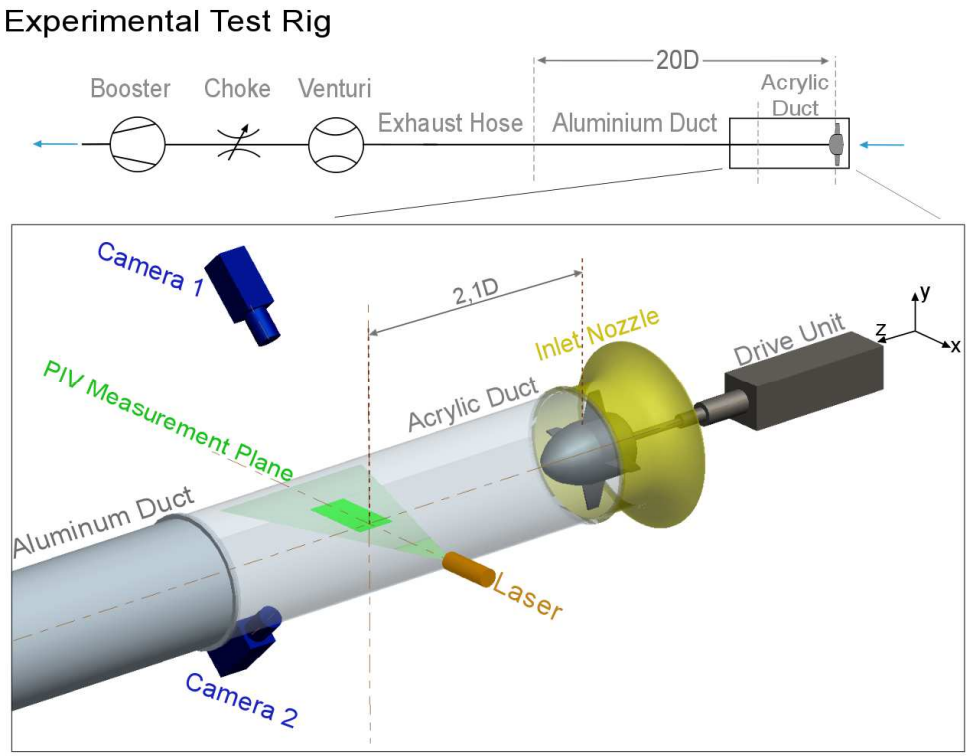

Figure 1: Experimental test rig, setup for measurements in x-z plane

In this study, Prof. Dr.-Ing. Z. Protić's† variable pitch fan was used as a swirl generator. The axial fan with nine blades had been designed with $r \cdot c_u = const.$ to be used with an outlet guide vane. The impeller diameter is $D_a = 0.399\ m$ with a tip clearance of *1,5 mm* and the dimensionless hub ratio $\nu = D_{Hub}/D_a = 0.5$ (see Figure 2). The blade angle at $D_a$was set to $\beta_a = 30°$.

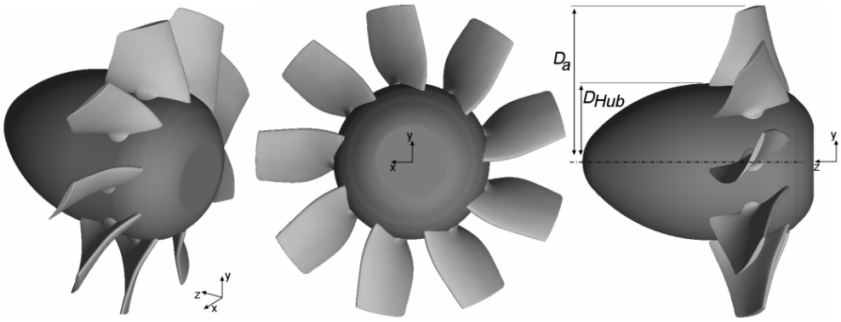

Figure 2: Axial fan impeller geometry, hub ratio v=0.5

HSS-PIV measurements

HSS-PIV measurements are carried out inthex-y and a x-z plane, both *2.1D* downstream of the fan's trailing edge, as defined in Figure 3.

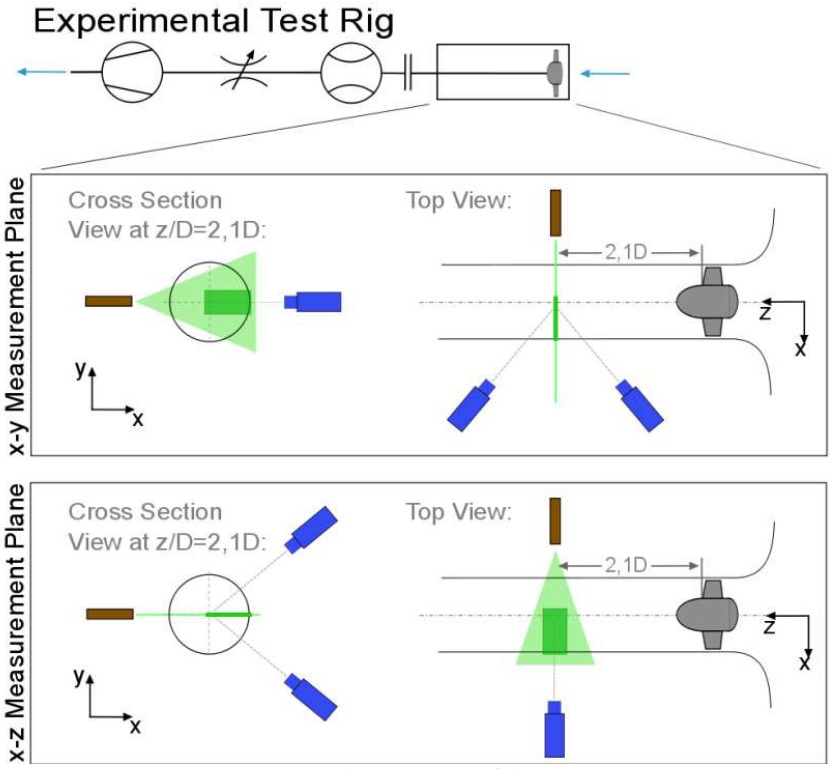

Figure 3:Position and orientation of the HSS-PIV setup

For flow illumination, a dual oscillator-single head, diode pumped Nd:YLF laser Darwin Duo from Quantronix©, with an output wavelength of 527nm is used. Two high speed cameras, Photron© FASTCAMSA4, with a 1008x1024 pixel resolution at 4000fps and the corresponding Photron© FASTCAM Viewer software are used for recording. Scheimpflug Tilt Adapters and two Canon© EF 85mm f/1.8 USM lenses on automated EOS Rings fromILA© GmbH have been used. The seeding was produced by an Antari© Z3000 fog machine loaded with Eurolite Smoke Fluid "-X- Extrem A2"
The postprocessing was realised by using PIVTEC©'s PIVView Version 3.2. Common methods of de-warping, disparity correction were applied. The cross correlation had an interrogation area of 32x32 pixels and an overlap of 50%.

EXPERIMENTAL RESULTS

For the characteristic curve of the fan, the wall pressure at *z/D=2.2* downstream of the blades' trailing edge was measured. In addition, the flow rate and ambient conditions were recorded. The resulting axial fan's characteristic curve is plotted in Figure 4. In the following presentation of the PIV results, three operation points at a rotational speed of *n=1200 rpm* are investigated which are marked by the green circles at the characteristic curve below.

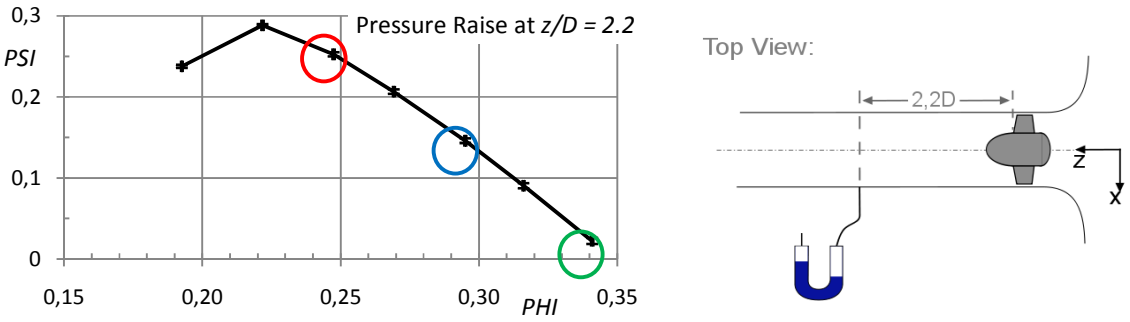

Figure 4:Characteristic curve of the fan (left), position of the pressure measurements (right)

HSS-PIVexperimental results

First the results for the x-y and x-z-plane at the operational point of *PHI=0.248* (Figure 4, left, red circle) will be illustrated before comparing all measured operating points. Here the distributions of the time-averaged velocity fields are plotted (average of around 2800 correlations). All velocities correspond to a cylindrical coordinate system and were made non dimensional by the averaged value of the axial velocity :

(1)

For the later applied product of the circumferential velocity and the radial position *r*, additionally the outer radius of the fan is used to clear the dimension: .
In the plots two black lines visualize the outer diameter of the hub D_{Hub} (at *x/D=0.25*) and duct *D* (at *x/D=0.5*).

Figure 5 shows that the results consist of two partially overlapping measurement areas, each surrounded by a red frame.

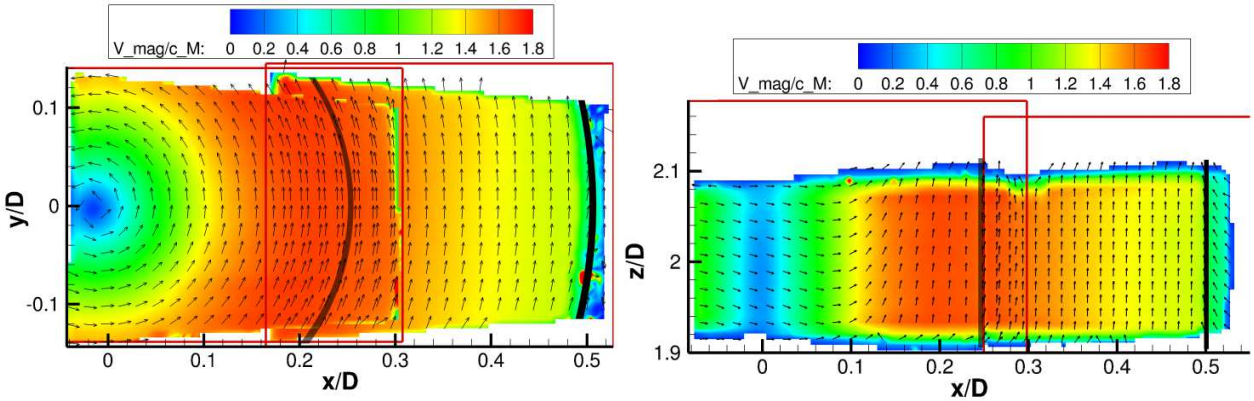

Figure 5: Average plot of the dimensionless velocity magnitude and vector field in the x-y and x-z plane, PHI=0.248

Furthermore Figure 5 illustrates the scalar of the velocity magnitude superposed by the vectors of the entire flow field. In the x-y plane (Figure 5, left) this vector field shows a uniform swirl flow, rotating counter clockwise corresponding to the rotational direction of the fan.

In the x-z plane (Figure 5, right) velocity vectors for *r/D=0.2* represent the expected axial flow downstream. At the vortex core region *-0.1<r/D<0.1* the flow seems to be directed in positive *x* direction, however the absolute value of the velocity is small. The reason for this is that the position of the measurement plane is not perfectly setup at *y/D=0* but slightly above. The velocity magnitude's minimum is situated in the core of swirl and its maximum of around *=1.7*is located at a radial distance of *r/D=0.22*.

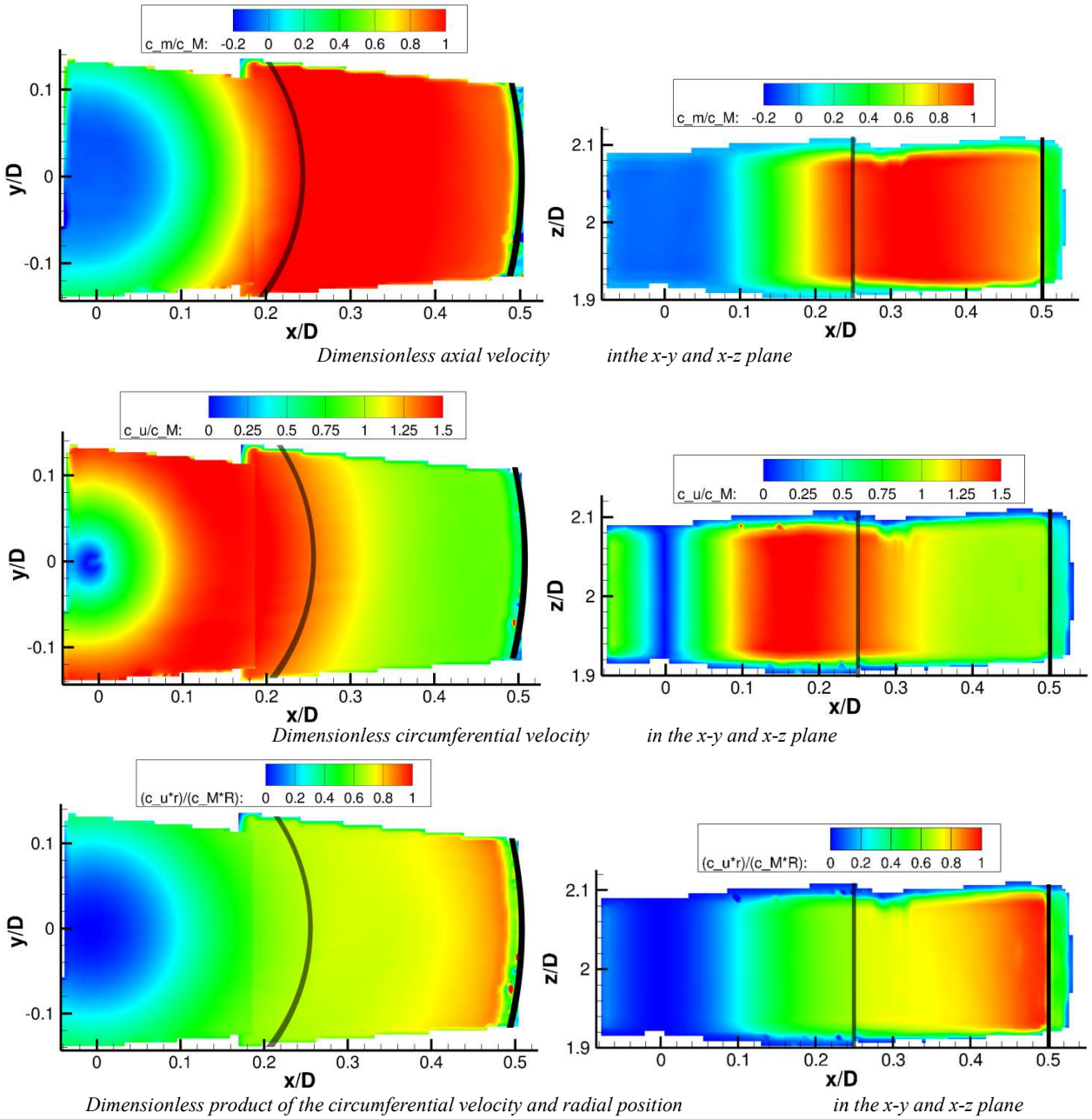

Dimensionless axial velocity inthe x-y and x-z plane

Dimensionless circumferential velocity in the x-y and x-z plane

Dimensionless product of the circumferential velocity and radial position in the x-y and x-z plane

Figure 6: Average plot of the dimensionless velocities at PHI=0.248

In the first row of Figure 6 the axial velocity is visualized. It is slightly negative (=*-0.1*) in the center and rises with increasing radial coordinate *r*. At a radius of *r/D=0.25* it reaches its maximum of almost and stays constant until *r/D=0.4*.Closer to the outer wall of the duct it decreases again to *r/D=0.5*.

The circumferential velocity is presented in the second rowof Figure 6. The minimum =*0* is found in the center of the swirl. With rising radial coordinate *r/D* it linearly reaches its maximum of =*1.5* at *r/D=0.15* and afterwards decreases to around =*0.8* close to the wall of the duct.

Additionally in row number three the product of circumferential velocity and radial tion is shown. The most interesting point here is the constant value of = *0.7* at *0.27 > r/D > 0.37*.

Since a rotational symmetric behavior of the flow could be proved (see Figure 6), the results of c_u and are further investigated in the 1D plot of Figure 7. For both measurement positions of the x-z-plane (Figure 7: left side in green Position 1 and 2) a 1-dimensional spline is extracted. As both measurements positions 1 and 2 were not perfectly overlaid, the resulting shift of the 1D splines (for c_u brown to red curve, for $c_u r$ blueto turquoise) were corrected, as Figure 7 right shows.

This 1D plot of and illustrates a Rankin vortex like behavior of the flow. An almost linear increase of the circumferential velocity from vortex core (red dashed line, Figure 7, right) changing over to a transition area including the maximum peak =*1.5* before declining again. The decline reaches a slope proportional to *~1/(r/D)* shortly after passing the radial distance of D_{Hub}, illustrated by a constant value of =*0.68* at *0.27 > r/D > 0.37* (blue dashed line, Figure 7, right).

Hence the forced vortex region is detected by the constant slope of followed by the transition area before changing over to the free vortex swirl at constant . Afterwards the influence of the wall starts changing the vortex characteristics.

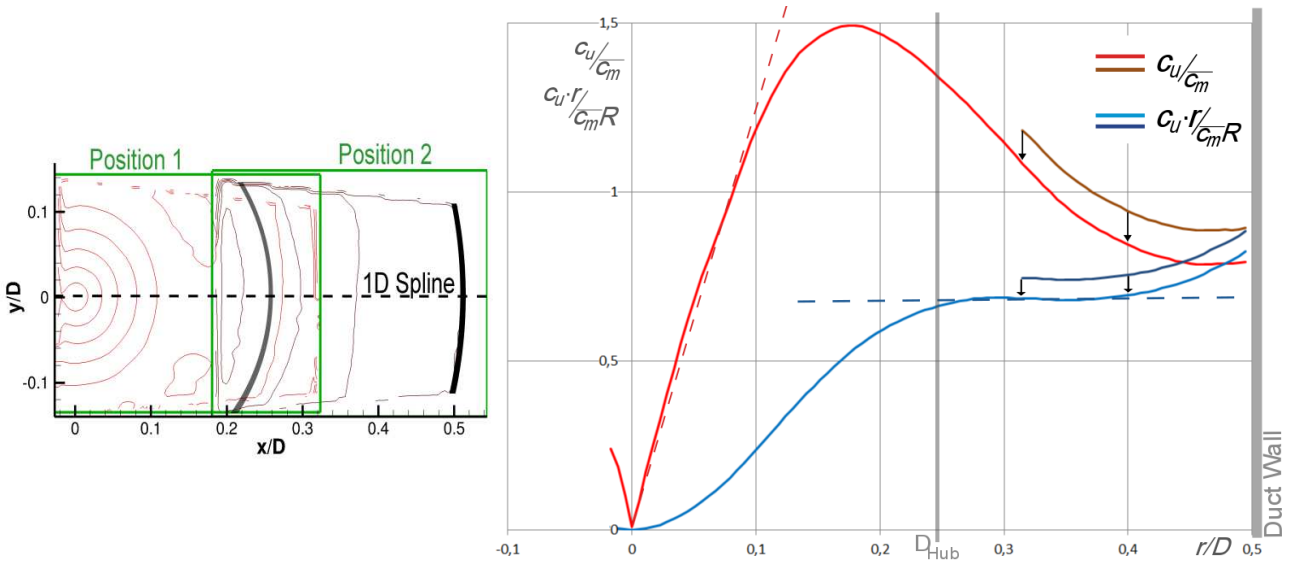

Figure 7: Extracted 1D spline for both measurement positions 1 and 2 (left), Rankine vortex behavior (right).

To summarize the results, Figure 8 is introduced. It shows the radial distribution of all velocity components comparing all three measured operating points (shown before in Figure 4).

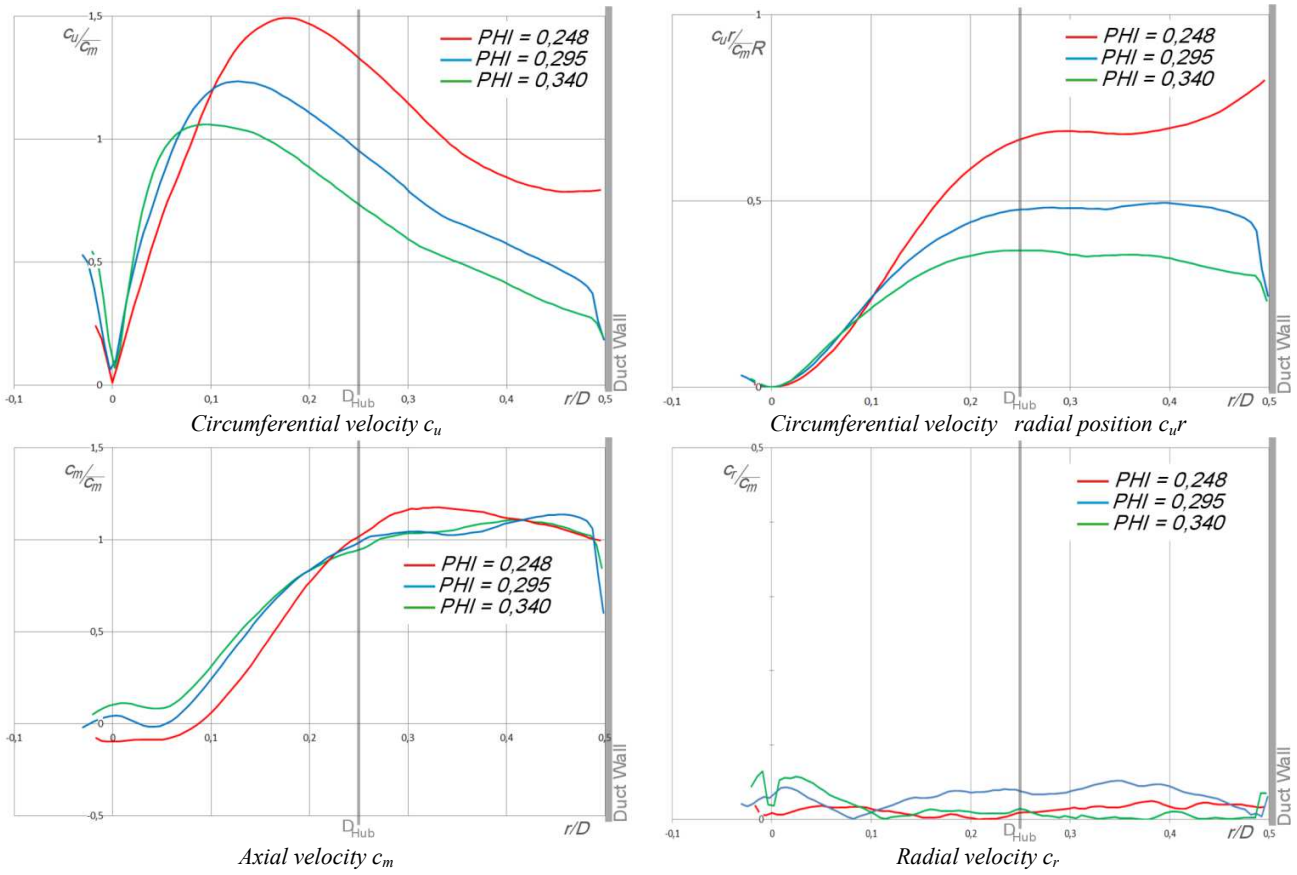

Figure 8: Summary of all velocity components comparing three operation points at z/D=2.1

Figure 8 shows for and , the maximum peak's value is shifted due to and hence the volume rate. Additionally the forced rotational vortex part decreases in its radial dimension *r/D* while the free rotational part grows in size. Here the distribution circumferential velocity shows the same trend. The reason is the reduced influence of the viscosity since the Reynolds number in the duct increases with rising volume flow: *Re*~ .

Generally the best point of the fan is expected between *PHI = 0.248* (red curve) and *PHI = 0.295* (blue curve), which could explain the different tendencies of the lowest volume flow (red curve) compared to the other two (blue and green curve), i.e. for at *r/D*> *0.4* respectively the distribution.

As expected from theory, for an impeller design of $r \cdot c_u = const$, the radial velocity c_r should be zero.

ANALYSIS

Analysis of the adequate loss allowances for straight circular pipe

The Darcy relation (2) treats the flow energy change in a fully developed axial flow,

(2)

where λ is a friction factor for axial flow, $z^*=z/R$ is a non-dimensional pipe length measuring from the test rig inlet and the averaged axial velocity of pipe flow.

The authors assume that the flow energy change for the swirl flow $\bar{Y}_{t\Gamma}$ can be written in a similar form:

$$\frac{d\bar{Y}_{t\Gamma}}{dz^*} = \lambda_\Gamma \frac{{U_m}^2}{4} \tag{3}$$

Where λ_Γ is the energy loss coefficient for a swirling flow along a straight circular duct.

Further analysis in paper [3] has shown that the swirl flow energy loss coefficient for a swirl flow along a straight circular pipe λ_Γ follows the expression:

$$\frac{\lambda_\Gamma}{\lambda} = 1 + 1.82\,{\Omega_0}^{-1.985} \cdot \exp\left(-14.95 \cdot 10^{-3} \cdot {\Omega_0}^{-0.418} \cdot {\Phi_0}^{-0.048} \cdot z^*\right) \tag{4}$$

With the swirl parameter $\Omega_0 = \Omega(z^* = 0)$ defined as:

$$\Omega = \frac{\dot{V}}{R\bar{\Gamma}} \quad \text{, and} \quad \bar{\Gamma} = \frac{4\pi^2}{\dot{V}} \int_0^R c_m c_u r^2 dr \tag{5}$$

Φ_0 is a similarity factor of any swirling flow with swirling flow of constant circulation.

Now, the authors introduced the swirl parameter W as:

$$W = \frac{4M_W}{\pi\rho {U_m}^2 D^3} \tag{6}$$

where M_W is the angular momentum:

$$M_W = \int_0^R c_m c_u r^2 dr \tag{7}$$

Bakerand Sayre (1974) [4] obtained the expression for a related energy loss coefficient $\frac{\lambda_\Gamma}{\lambda}$ for the Reynolds number in the range $1.25 \cdot 10^4 \leq \mathrm{Re} \leq 2 \cdot 10^5$ by:

$$\frac{\lambda_\Gamma}{\lambda} = 1 + 11.5\,{W_0}^{1.32} \cdot \exp\left(-0.4b\frac{L}{D}\right) \tag{8}$$

where b is a decay parameter first introduced in the relation for exponential decay of the swirl parameter W in the same paper. Relation (8) is valid for flow between two points up to the maximum distance $L=20D$. $\frac{\lambda_\Gamma}{\lambda}$ is only a weak function of Re and is mainly dependent on the initial swirl parameter W_0.

The authors obtained relation (4) for a wider range of Reynolds numbers and a larger distance which was comparable to the relation (8) as $W_0 \sim {\Omega_0}^{-1}$.

Analysis of pressure distribution on the wall

On the basis of the investigations for turbulent swirl flow [2], we can conclude that in an optimal case for ν=0.5, the wall pressure reaches its maximum quickly, on the distance of $D=0.5$. We can apply this in the case of adopting ISO 5801 Chapter 28.4 “Outlet duct simulation”. Additional research is necessary in order to find dependence for non-optimaloperating points.

CONCLUSIONS

The performed experiments have proven the complexity of the turbulent swirl flow field, its three-dimensionality, anisotropy and non-homogeneity. The obtained results have shown good agreement with classical methods.

The velocity distribution of the turbulent swirl flow in a straight duct behind an axial fan without outlet guide vanes varies under the influence of internal andwall friction [6]. HSS-PIV measurements show great vortex core dynamics and the possibility to successfully delve deeper into the turbulent flow field in the vortex core region, an area almost impossible to reach with hot-wire anemometry probes.

The distribution of the circumferential velocity obeys the constant circulation law not only short behind the fan (which is designed with $r \cdot c_u = const.$), as shown in this paper, but also in cross sections in more than *20D* distance to the fan [6, 7]. The authors in [6] conclude that only the intensity, and not the character of the constant circulation profile has changed under the influence of friction.

The relation for the flow energy loss coefficient in a straight circular duct (Eq. 4) shows significant influence on the swirl parameter in the starting cross section. One could obtain the fan pressure of an axial fan without outlet guide vanes in category B setups just by determining the related wall pressure downstream of the fan, without "common-segment airways" specified in Chapter 28.2 of ISO 5801, calculating loss allowances according to the Eq. (4). But for that additional measurement information is necessary.A trusted proposal for a change in ISO5801 in this point requires further investigations. They can relate the missing informationto the length of the "Carnot annular diffuser" and the maximum of the wall pressure.

ACKNOWLEDGMENTS

This work was funded by grants from the Ministry of Education and Science, Republic of Serbia (Project TR 35046), the bilateral project with German Academic Exchange Service (DAAD) "*Investigation of the Turbulent Structure behind the Axial Fan Impellers by Use of the HWA, LDAand PIV Measuring Techniques and CFD Analysis"* and a cooperation of the Faculty of Mechanical Engineering, Karlsruhe Institut of Technology and the Faculty of Mechanical Engineering, University of Belgrade.

BIBLIOGRAPHY

[1] ISO 5801 – *Industrial fans –Performance testing using standardized airways*, **2007**

[2] D. Vasilescu –*A Contribution to the swirl flow in the pipe behind the sudden transition from anannular in a circular cross section (in German),* PhD thesis, Fac. of Mech. Eng., TechnicalUniversity Karlsruhe, Karlsruhe, **1977**

[3] M. Benišek, S. Čantrak, M. Nedeljković – *An investigation on the changes of Coriolis and energy loss coefficients for a swirling flow along straight circular pipes*, Z. Angew. Math. Mech.,74 (5), T 349-T 351, **1994**

[4] A. Ward-Smith – *Internal fluid flow - The fluid dynamics of flow in pipes and ducts*, Clarendon-press, Oxford, **1980**

[5] S. Čantrak, K.O. Felsch, H. Jungbluth – *Turbulence structure and mechanism of the transportprocess in turbulent swirl flow in diffusers(in German)*, Z. Angew. Math. Mech., 65 (4), T 189-T191, **1985**

[6] Z. Protić, M. Benišek, M. Manasijević – *Swirling flow in the circular pipes – the characteristicvalues and flow-patterns specifics*, Z. Angew. Math. Mech., 71 (5), T 456-T 459, **1991**

[7] Đ. Čantrak, M. Nedeljković, N. Janković - *Turbulent swirl flow dynamics*, Proceedings of the 3rdInternational Congress of Serbian Society of Mechanics, Vlasina Lake, Serbia, **2011**